Highly-Efficient Degradation of Ensulizole using Monopersulfate activated by Nanostructured Cobalt Oxide: A Comparative Study on Effects of Different Nanostructures

Wei-Jie Liu[a], Young-Kwon Park[b], Wei-Hsin Chen[c,d,e], Ha Manh Bui[f], Venkata Subbaiah Munagapati[g], Duong Dinh Tuan[a], Jet-Chau Wen[g,h], Siming You[i], Wen Da Oh[j,], and Kun-Yi Andrew Lin[a,*]*

[a]Department of Environmental Engineering & Innovation and Development Center of Sustainable Agriculture, National Chung Hsing University, 250 Kuo-Kuang Road, Taichung, Taiwan

[b]School of Environmental Engineering, University of Seoul, Seoul 02504, Republic of Korea

[c]Department of Aeronautics and Astronautics, National Cheng Kung University, Tainan 701, Taiwan

[d]Research Center for Smart Sustainable Circular Economy, Tunghai University, Taichung 407, Taiwan

[e]Department of Mechanical Engineering, National Chin-Yi University of Technology, Taichung 411, Taiwan

[f]Department of Environmental Sciences, Saigon University, Ho Chi Minh, 700000, Vietnam

[g]Research Center for Soil & Water Resources and Natural Disaster Prevention (SWAN), National Yunlin University of Science and Technology, Douliou, Taiwan, Douliou, Taiwan

[h]Department of Safety, Health, and Environmental Engineering, National Yunlin University of Science and Technology, Douliou, Taiwan

[i]James Watt School of Engineering, University of Glasgow, Glasgow G12 8QQ, UK

[j]School of Chemical Sciences, Universiti Sains Malaysia, 11800 Penang, Malaysia

*Corresponding Authors. E-mail address: linky@nchu.edu.tw (K.-Y. A. Lin); ohwenda@usm.my (W. D. Oh)

Abstract

The most extensively used sunscreen protecting agent, Ensulizole, has been proven to exhibit hormone disrupting effects. To establish efficient processes to destruct Ensulizole in water, $SO_4^{\bullet-}$-involved advanced oxidation processes using monopersulfate (MPS) seem useful. Since cobalt (Co) is the most capable of metal for activating MPS, Co_3O_4 appears as a promising heterogeneous catalyst for activating MPS to degrade Ensulizole. As catalytic activities of metal oxide catalysts are strongly associated with their morphologies, and surficial properties, nanoscale Co_3O_4 with functional nanostructures would be expected as advantageous catalysts for activating MPS. Therefore, three Co_3O_4 materials with distinct nanostructures and shapes were fabricated in this study, including Co_3O_4 cone ball (COCB), Co_3O_4 plate lump (COPL), and Co_3O_4 needle sheaf (CONS). Their surficial properties are also noticeably distinct with different fractions of Co^{2+}, and Co^{3+}, various oxygen vacancies, textural features and surface defects. Through comparing these three nanostructured Co_3O_4 for activating MPS to degrade Ensulizole, CONS exhibits the tremendously higher catalytic activity than COCB and COPL for activating MPS to eliminate Ensulizole completely and rapidly. The E_a value of Ensulizole degradation of CONS is also significantly low as 9.8 kJ/mol, which is the lowest E_a ever reported in literatures. CONS could also retain its catalytic activities over 5 continuous cycles to rapidly degrade Ensulizole. The activation mechanism of MPS by CONS and Ensulizole degradation pathway are also comprehensively elucidated via experimental evidences and the theoretical calculation to offer insightful information of development of Co-based heterogeneous catalysts for Ensulizole degradation.

Keywords: UV filter, sunscreens, cobalt, Ensulizole, Oxone, nanostructure

1. Introduction

Sunscreen protecting agents (SPAs) have been widely consumed nowadays for guarding skin from UV irradiation. While various types of SPAs are available, Ensulizole has been recognized as the most extensively used SPA especially because Ensulizole can efficiently adsorb UVB irradiation, and also frequently coupled with other reagents for preventing UVA irradiation [1, 2]. Nonetheless, Ensulizole has been listed as an emerging contaminant due to its endocrine disrupting effects [3, 4]. Therefore, discharge of this water-soluble Ensulizole into water would cause serious threats to the environment and ecology, and it is highly crucial to establish efficient processes to destruct Ensulizole in water. Specifically, Ensulizole has been continuously detected in various water systems. For example, Ensulizole has been found in both influent and effluent of anaerobic and aerobic gray water treatment systems with its concentration could be *ca.* of 4.9 μg/L [5] whereas the concentration of Ensulizole about 1.8~836.3 ng/L has been also detected in surface waters [6].

As advanced oxidation processes (AOPs) are generally considered as useful treatments for treating organic contaminants, AOPs have been also demonstrated to eliminate emerging contaminants. While AOPs are usually involved with various radicals (e.g., $^{\bullet}OH$) and reactive oxygen species (ROS), recently $SO_4^{\bullet-}$-involved AOPs also draw growing attention because $SO_4^{\bullet-}$ exhibits higher oxidation power, longer half-lives as well as higher selectivities [7-12]. Therefore, $SO_4^{\bullet-}$-involved AOPs shall be promising and useful for eliminating Ensulizole. For obtaining $SO_4^{\bullet-}$, monopersulfate (MPS) represents the most common reagent because MPS is commercially available, easily accessible, environmentally benign and inexpensive [13-16]. However, generation of $SO_4^{\bullet-}$ from MPS itself is sluggish and inefficient; thus, MPS must be activated to quickly decompose MPS into $SO_4^{\bullet-}$. For instance, Zhang and his co-colleagues investigated

Ensulizole degradation using NS-CNTs/$CuFe_2O_4$ coupled with monopersulfate [4]. Besides, Yin et al. prepared MOF-derived cobalt sulfide nanoplates for monopersulfate activation to degrade Ensulizole in water [17].

Among various activation methods, usage of metal catalysts for activating MPS has been validated as the most practical one, and cobalt (Co) is the most capable metal for activating MPS [16, 18-22]. However, the direct addition of Co ions into solutions would cause several issues, such as difficult recovery of Co ions, and secondary pollution [23, 24]. Therefore, cobalt oxides (e.g., Co_3O_4) are already recognized as the most suitable heterogeneous catalyst to substitute Co ions [19, 25, 26]. Unfortunately, very few studies have been ever reported by using Co_3O_4 for activating MPS to degrade Ensulizole. Moreover, since catalytic activities of metal oxide catalysts are strongly associated with their morphologies, surficial properties and other physio-chemical features, nanoscale Co_3O_4 with functional nanostructures would be expected as advantageous catalysts for activating MPS [7, 27-31]. Therefore, it would be critical to explore how nanostructured Co_3O_4 with different morphologies, and characteristics would behave to activate MPS in order to optimize the design and fabrication of Co_3O_4 catalysts for activating MPS in Ensulizole degradation.

Nonetheless, almost no such a study has ever been conducted so far to look into the relationship between shapes, surficial properties and nanostructures of Co_3O_4 materials, and their catalytic activities for MPS. Therefore, the goal of this study is aimed to develop various nanostructured Co_3O_4 and investigate these Co_3O_4 for activating MPS to degrade Ensulizole. Specifically, three Co_3O_4 materials with distinct nanostructures and shapes were fabricated, including Co_3O_4 cone ball (COCB), Co_3O_4 plate lump (COPL), and Co_3O_4 needle sheaf (CONS), and investigated for their catalytic activities of MPS activation.

To conduct Ensulizole degradation experiments, batch-type experiments were employed, in which different parameters influencing Ensulizole degradation were examined including catalyst dosage, MPS dosage, temperatures, pH values and different water sources. The existence of ROS generated from Co_3O_4-activated MPS was verified by Electron Spin Resonance (ESR). The degradation pathway of Ensulizole is also elucidated based on the detected intermediates. By experimental and theoretical investigations, insightful behaviors and mechanisms of Ensulizole degradation by nanostructured Co_3O_4+MPS system are further elucidated.

2. Experimental

The preparation procedure of various nanostructured Co_3O_4 is illustrated schematically in Fig. 1(a). In general, Co^{2+} from different cobalt salts would be mixed with carbamide in either ethylene glycol and DI water, and the resulting mixture would be hydrothermally processed, followed by calcination to afford various nanostructured Co_3O_4. The comprehensive preparation protocols, material characterizations and tests of Ensulizole degradation were given in the supporting information (SI).

3. Results and discussion

3.1 Characterizations of nanostructured Co_3O_4

As these Co_3O_4 catalysts were prepared using different cobalt salts, concentrations of carbamide and solvents, distinct morphologies of Co_3O_4 would be evolved. Fig. 1(b-d) reveal the actual morphologies of the as-prepared Co_3O_4, whereas Fig. S1 displays precursor images of these Co_3O_4 before the calcination. Specifically, the resultant product displayed in Fig. 1(b) shows a ball-like substance with a microscale diameter. More interestingly, the surface of this ball-like product was

comprised of many conic structures whose sizes were a few hundreds of nanometers. Its TEM image (Fig. 2(a)) also indicates that this resultant product was solid with the rounded edge.

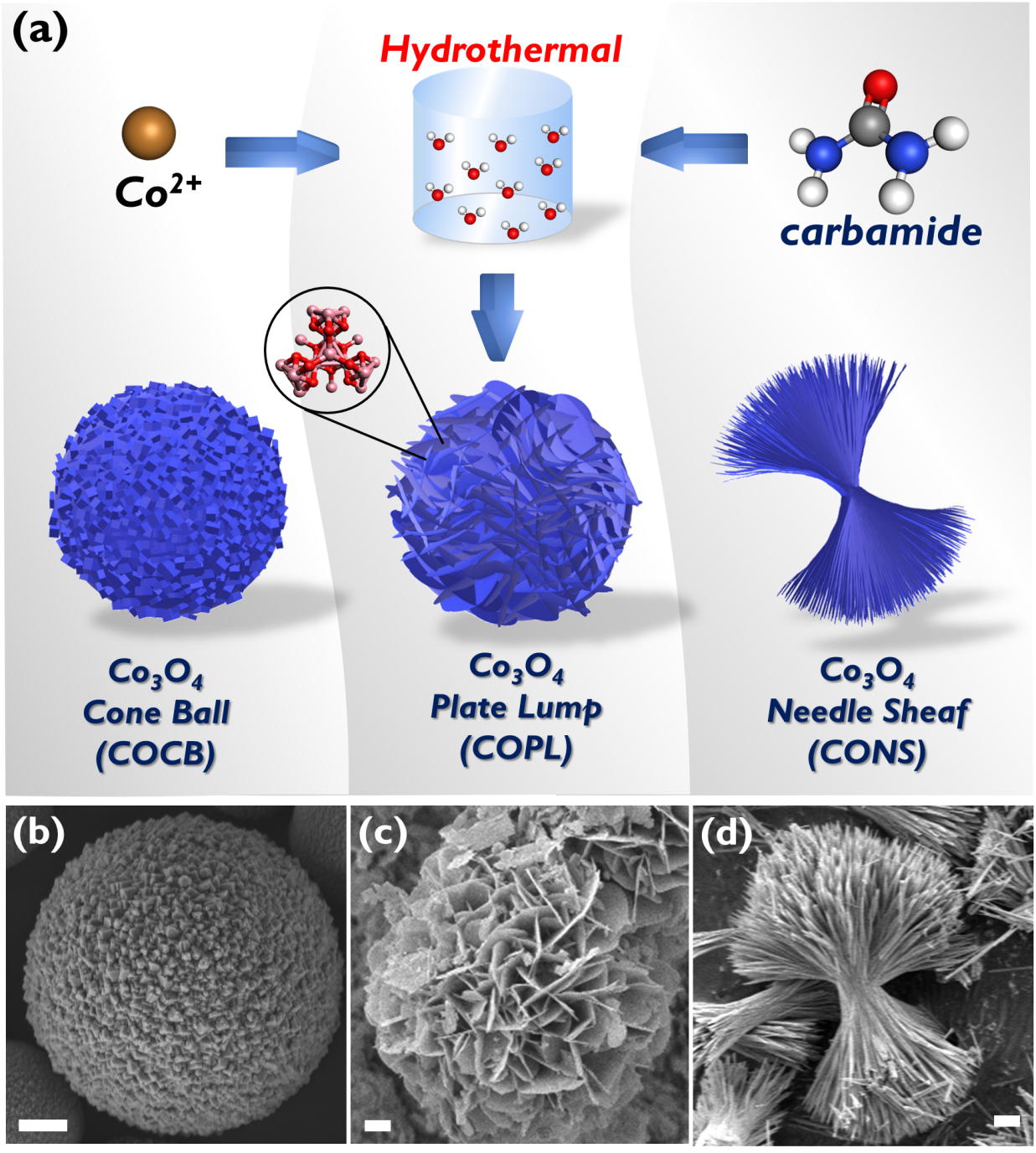

Fig. 1: (a) Scheme for preparing nanostructured Co_3O_4; SEM images of (b) COCB, (c) COPL, and (d) CONS (the scale bar is 1 μm).

Secondly, Fig. 1(c) displays the product derived from the hydrothermal process of using cobalt nitrate and carbamide in ethylene glycol, and its morphology seemed a lump comprised of many plates inter-penetrated. The size of this lump was also around 10 μm; however, the thickness of these plates were a few tens of nanometers. Especially, the inter-penetrating configurations enabled this special product to exhibit voids. Fig. 2(b) also reveals that the plate in this product was very thin, and it was comprised of many fine particles. On the other hand, Fig. 1(d) shows the product from the hydrothermal process of $CoCl_2$ and carbamide in water exhibited a relatively distinct configuration in which needle-like substances with relatively high aspect ratios were bundled to afford a morphology of sheaf. Fig. 2(c) also validated that these needle-like products were nanoscale with a few tens of nanometers in diameter, and it was also comprised of many fine particles.

To further identify these products, their lattice-resolved HRTEM images were also listed in Fig. 2. Specifically, Fig. 2(d) reveals the lattice-resolved image of the product with the CB morphology, in which the (0-22), and (-202) plane of Co_3O_4 with a *d*-spacing of 0.290 nm at an interfacial angle of 60°, could be detected. This suggests that this resulting product was Co_3O_4 [32]. Its corresponding SAED pattern (Fig. 2 (g)) can be well-indexed to Co_3O_4, confirming that this resultant material was Co_3O_4 with a polycrystalline structure [33, 34]. Thus, this resultant material could be confirmed as Co_3O_4 with CB morphology (COCB).

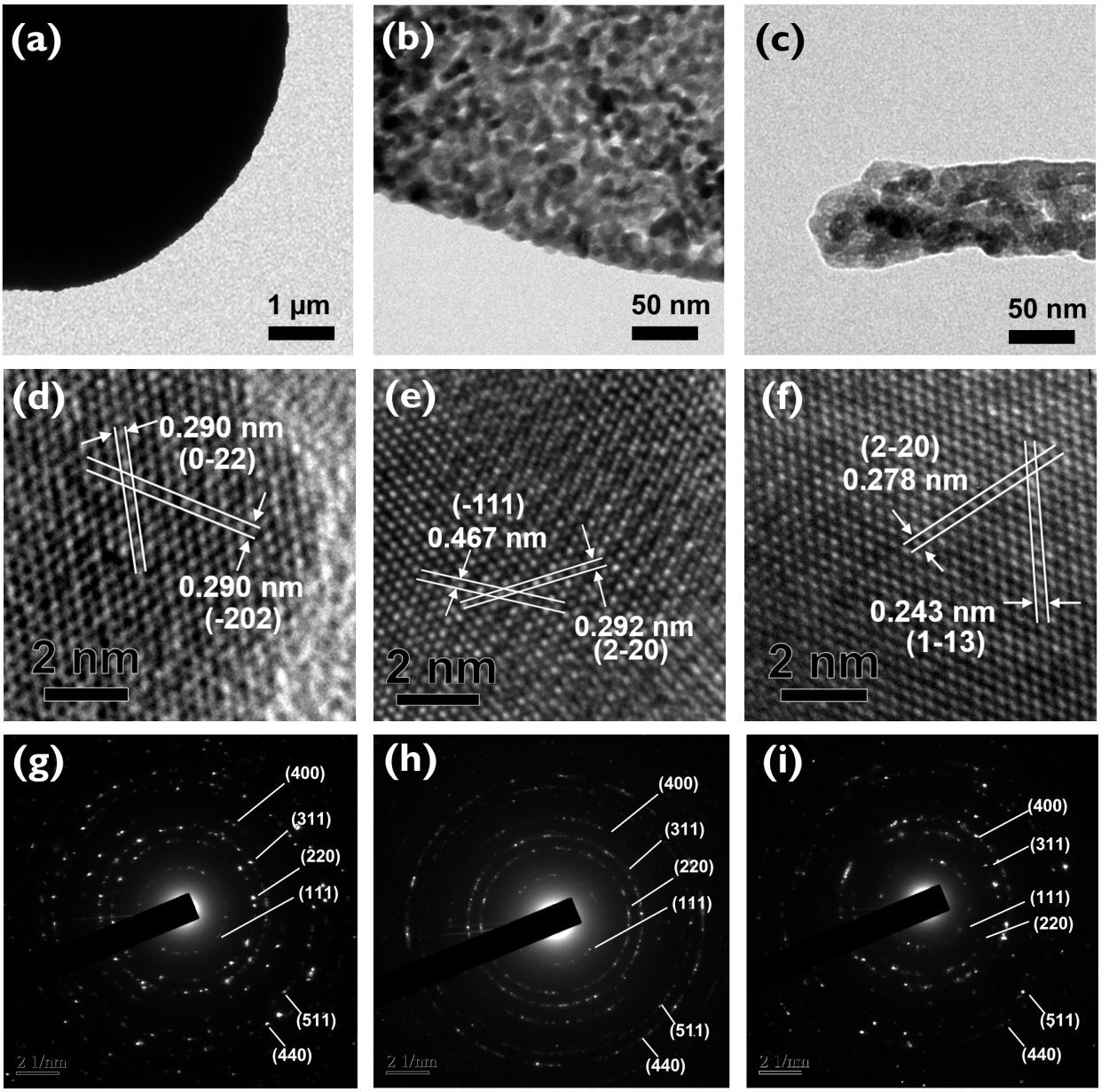

Fig. 2. TEM images of nanostructured Co_3O_4:(a) COCB, (b) COPL, and (c) CONS; HRTEM images of (d) COCB, (b) COPL, and (c) CONS; and SAED patterns of COCB, (b) COPL, and (c) CONS.

Besides, Fig. 2(e) unveils the lattice-resolved TEM image of the resultant material with the morphology of plate lump, in which the (-111) (*d*-spacing of 0.467 nm) and (2-20) (*d*-spacing of 0.290 nm) crystal planes of Co_3O_4 at an interfacial 45° was detected. This also confirms that the

successful formation of Co_3O_4 with the morphology of plate lump (COPL) [35]. Its corresponding SAED pattern could be also well-attributed to the poly-crystalline structure of Co_3O_4. On the other hand, Fig. 2(f) displays the lattice-resolved TEM image of the resulting product with the morphology of needle sheaf (NS), in which the (1-13), and (2-20) planes of Co_3O_4 at an interfacial angle of 65° were detected, indicating the formation of Co_3O_4 with the morphology of NS (CONS) [35]. The corresponding SAED pattern was also well-indexed to the polycrystalline structure of Co_3O_4.

The XRD patterns of these Co_3O_4 catalysts were also determined and summarized in Fig. 3(a), and all these patterns were well-indexed to the reported pattern of Co_3O_4 according to JCPDS #42-1467, validating that these resultant materials were Co_3O_4 with very distinct morphologies. The variation in morphology of nanostructures could be correlated to the anisotropic development of the self-agglomeration of crystallites [36], especially because morphologies of metal oxides would be attributed to the evolution of crystalline nuclei which would be then influenced significantly in the presence of additives (e.g., polymers, and surfactants) [36, 37].

Since an additive, carbamide, was particularly employed in the fabrication of Co_3O_4, carbamide would be readily hydrolyzed to produce carbon dioxide and ammonia [38]. Ammonia would be then transformed to NH_4^+ and OH^- upon exposing to water, and OH^- would react with Co^{2+} to form cobalt hydroxide. Furthermore, NH_4^+ would cause the reaction medium to be basic, and alter rates of cobalt hydroxide precipitate, thus manipulating the morphology. Moreover, the concurrently resulting carbon dioxide would also cause pressures to alter the development of nanocrystallites. Since various cobalt salts were adopted here, the corresponding counter anions of cobalt salts would also serve as template agents to manipulate crystalline nuclei [39]. Therefore, when lower amounts of carbamide were involved (such as COCB and COPL), the resulting

morphology of Co_3O_4 would be more like cones and plates. Nevertheless, a high amount of carbamide (such as CONS) was used, needle-like morphology would be afforded.

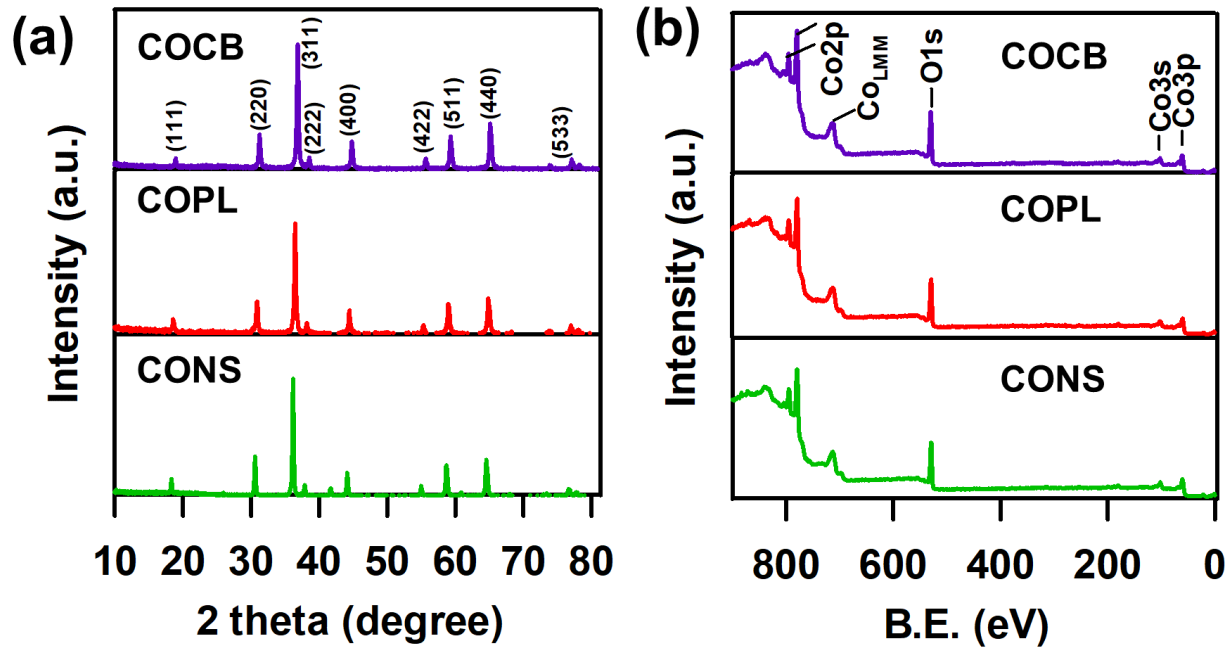

Fig. 3 Characteristics of nanostructured Co_3O_4: (a) XRD patterns, and (b) full-survey XPS spectra.

While these resultant materials were all proven to be Co_3O_4, it would be worthwhile to further investigate their surface chemistry as they exhibited very distinct shapes. Thus, XPS full-survey spectra of these Co_3O_4 were measured and displayed in Fig. 3(b), which exhibited very strong signals of Co and O in these materials, and no other noticeable elements could be found. Fig. 4(a) then reveals the Co2p core-level spectra of these nanostructured Co_3O_4 which exhibited very similar patterns with two noticeable broad bands in the ranges of 778~784 eV, and 792~800 eV, attributed to $Co2p_{3/2}$, and $Co2p_{1/2}$, respectively [40, 41]. Specifically, the $Co2p_{3/2}$ spectra could be deconvoluted to afford two bands at 780.1, and 781.7 eV, corresponding to Co^{3+} and Co^{2+} [42],

respectively, as these species are theoretically comprised in Co3O4. Nonetheless, the fractions of these two species might be influenced owing to slightly different surficial properties of Co3O4. Therefore, the percentages of Co^{2+}, and Co^{3+} of each nanostructured Co_3O_4 was determined in Table S1. Among these three Co_3O_4, CONS showed a relatively high percentage of Co^{2+}. Since Co^{2+} has been validated as a useful species to activate MPS [18], the relatively abundant Co^{2+} might enable CONS to exhibit a higher catalytic activity of MPS activation.

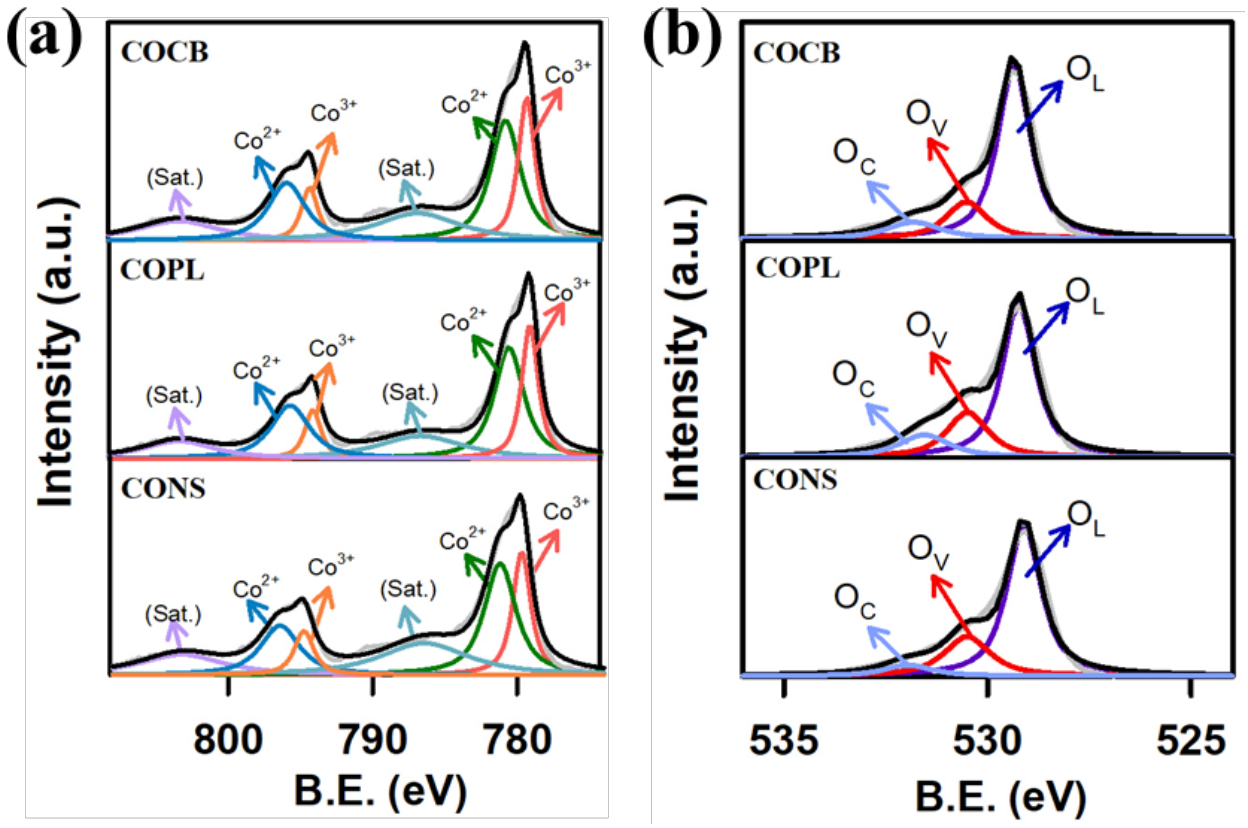

Fig. 4 (a) Co2p and (b) O1s core-level XPS spectra of nanostructured Co_3O_4.

On the other hand, the O1s core-level spectra of these nanostructured Co_3O_4 are displayed in Fig. 4(b), and these spectra could be also deconvoluted to exhibit three sub-bands located at ca. 529.3, 530.5, and 531.7 eV, corresponding to lattice oxygen (O_L), and oxygen vacancy (O_V), and

chemisorbed oxygen (Oc). Since OV has been validated to play a critical role in catalytic processes, and thus the fractions of O_V in these Co_3O_4 (as summarized in Table S1) would be also associated with their catalytic activities. In particular, the fraction of O_V in CONS was also slightly higher than other two Co_3O_4, suggesting the surficial characteristics of CONS were slightly distinct from those of these other Co_3O_4, and might behave differently in activating MPS to degrade Ensulizole.

Besides, Raman spectroscopic analyses of these nanostructured Co_3O_4 were also acquired to probe into their chemical structure in Fig. S2, and their spectra appeared very comparable to consist of 5 noticeable peaks. In particular, the peaks at 620, 523 as well as 194 cm^{-1} could be attributed to the F_{2g} symmetry of Co_3O_4 [43, 44]. Additionally, the peak at 485 cm^{-1} would be ascribed to the E_g symmetry of Co_3O_4, while the peak located at 694 cm^{-1} would be correlated to the A_{1g} symmetry of Co_3O_4 [45, 46]. More importantly, as the location of a certain Raman peak might be shifted owing to structural variation (i.e., defects), a noteworthy feature could be noticed that the A_{1g} symmetry peaks of these three nanostructured Co_3O_4 were slightly distinct as the A_{1g} peak center of CONS was shifted to the left side of the X-axis. This suggests that CONS might exhibit a higher degree of structural defect, which might enable the surface of CONS to be more reactive for improving its catalytic activities [47].

Aside from the aforementioned distinct surficial characteristics, these nanostructured Co_3O_4 essentially showed very different morphologies, and thus their textural properties should be further analyzed. Fig. S3(a) shows N_2 sorption isotherms of these nanostructured Co_3O_4, and CONS seemed to exhibit the highest N_2 sorption amount, followed by COPL, and then COCB. Therefore, COCB showed a relatively low surface area of 53 m^2 with a pore volume of 0.20 cm^3/g, whereas COPL could show a significantly higher surface of 75 m^2 with a pore volume of 0.30 cm^3/g, and

CONS showed a specific surface area of 106 m^2 with a pore volume of 0.32 cm^3/g. This indicates that the distinct appearances of these Co_3O_4 materials would lead to very different textural features, which were anticipated to govern their catalytic behaviors upon exposing to MPS and Ensulizole.

On the other hand, since the study was to investigate the degradation of Ensulizole by MPS in water, another surficial property, surface charge, of these Co_3O_4 would also play an important role in contact with MPS/Ensulizole. Thus, the surface charges of these Co_3O_4 would be measured and displayed in Fig. S3(b), and generally, their surface charges exhibited a trend that the surface charge would gradually become more negative at higher pH values. In addition, pH_{pzc} of these Co_3O_4 catalysts were ranged from 6 to 8.

3.2 Catalytic degradation of Ensulizole by Co_3O_4-activated MPS

Fig. 5(a) further displays Ensulizole degradation using MPS activated by these nanostructured Co_3O_4. Since Ensulizole might be removed through adsorption to Co_3O_4, adsorptive tests had been also conducted in Fig. 5(a). Nevertheless, almost these Co_3O_4 catalysts were incapable of removing Ensulizole through adsorption. On the other hand, MPS itself was also tested to examine whether the self-decomposition of MPS could degrade Ensulizole. Fig. 5(a) indicates that while Ensulizole could be slightly degraded with C_t/C_0 at 60 min (C_{60}/C_0) approaching 0.8, such an efficiency was quite low, and thus MPS itself was still incapable of removing Ensulizole. Nevertheless, once COCB was combined with MPS, Ensulizole was quickly degraded and C_{60}/C_0 would approach 0.35. Because COCB and MPS were incapable of removing Ensulizole individually, this result suggests that COCB could activate MPS to generate reactive oxygen species to attack Ensulizole.

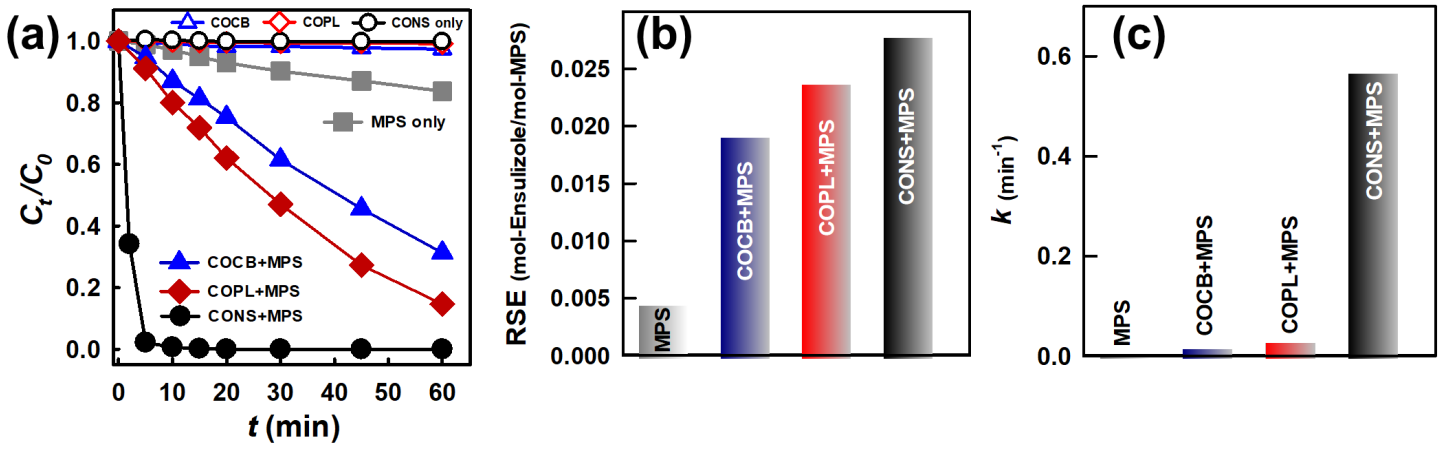

Fig. 5 Activation of MPS by various nanostructured Co_3O_4 for degradation of Ensulizole: (a) comparisons between adsorption to Co_3O_4, MPS and Co_3O_4 + MPS, (b) RSE, and (c) rate constants (Co_3O_4 catalysts = 100 mg/L, MPS = 100 mg/L, T = 30°C)

On the other hand, COPL coupled with MPS was also found to degrade Ensulizole as C_{60}/C_0 would approach 0.15. This result demonstrated that COPL could also activate MPS to degrade Ensulizole, and COPL seemed to exhibit a higher catalytic activity than COCB to activate MPS. Furthermore, once CONS was combined with MPS, Ensulizole was rapidly degraded and C_{60}/C_0 reached to zero in 10 min. This surprising result not only suggested that CONS could activate MPS for degrading Ensulizole but also the catalytic activity of CONS towards MPS activation. While these nanostructured Co_3O_4 were comprised of almost identical chemical compositions, their activities towards MPS activation were significantly distinct. Since these nanostructured Co_3O_4 catalysts exhibited distinct catalytic activities for activating MPS to degrade Ensulizole, it would be beneficial to measure the mineralization degree of Ensulizole using the total organic carbon (TOC). As depicted in Fig. S4, different TOC results were obtained by these catalysts. Specifically, ca. 65% of TOC was achieved by CONS+MPS system, followed by COPL+MPS (50%) and COCB+MPS (42%), respectively. This result indicated that Ensulizole was certainly decomposed

by these nanostructured Co_3O_4 catalysts-activated MPS; however, CONS showed higher mineralization degree compared to COPL and COCB.

For further quantifying the differences in activity of these nanostructured Co_3O_4 for degrading Ensulizole, reaction stoichiometric efficiency (RSE) has been adopted to describe activities of catalysts for activating MPS to degrade organic contaminants through the following equation [48, 49]:

$$\text{Reaction Stoichiometric Efficiency (RSE)} = \frac{\text{Ensulizole degraded (mol)}}{\text{MPS added (mol)}} \quad (1)$$

The RSE at 60 min obtained by MPS, and combinations of these nanostructured Co_3O_4 and MPS were displayed in Fig. 5. While the RSE of MPS was extremely low as 0.004, RSE of the combinations of these nanostructured Co_3O_4 and MPS were much higher. As CONS could completely eliminate Ensulizole in 60 min, CONS exhibited the highest RSE as 0.027, followed by COPL with a RSE of 0.024, and then COCB with a RSE of 0.018. This comparison indicates that these nanostructured Co_3O_4 were all capable of activating MPS to degrade Ensulizole; nevertheless, CONS showed a much higher capability for activating MPS. On the other hand, while RSE could be an index to reveal degradation efficiency, it would also require another index to interpret the reaction kinetics especially because CONS could lead to the extremely fast degradation of Ensulizole.

To describe the degradation kinetics, the pseudo first-order rate law was then adopted because it has been widely employed for determining the kinetics of pollutant degradation using MPS as follows [50]:

$$\ln(C_t/C_0) = -kt \quad (2)$$

where k denotes as the pseudo first-order rate constant. Fig. 5(c) shows the calculated k values of Ensulizole degradation by MPS, COCB+MPS, COPL+MPS, and CONS+MPS. Even though

COPL+MPS and COCB+MPS could also lead to Ensulizole degradation, their *k* values were actually quite low as 0.0318 and 0.0195 min^{-1}. In contrast, the *k* value obtained by CONS was significantly higher as 0.567 min^{-1}. This kinetic analysis demonstrated that CONS was surpassingly more powerful than COPL and COCB for activating MPS to degrade Ensulizole swiftly.

As nanostructured Co_3O_4 catalysts were all comprised of Co^{2+}, and Co^{3+} species, these Co species can activate MPS to produce ROS ($SO_4^{\bullet-}$, $^{\bullet}OH$) through following equations [51]:

$$Co^{2+}@Co_3O_4 + HSO_5^- \rightarrow Co^{3+}@Co_3O_4 + SO_4^{\bullet-} + OH^- \quad (3)$$

$$Co^{3+}@Co_3O_4 + HSO_5^- \rightarrow Co^{2+}@Co_3O_4 + SO_5^{\bullet-} + OH^- \quad (4)$$

$$SO_5^{\bullet-} \rightarrow SO_4^{\bullet-} + 1/2O_2 \quad (5)$$

According to these reactions, Co^{2+} seemed to play a more important role than Co^{3+} to quickly generate the more reactive species, $SO_4^{\bullet-}$ for attacking Ensulizole. As CONS contained a relatively high fraction of Co^{2+}, it was expected to enable the quicker decomposition of MPS into $SO_4^{\bullet-}$, thereby leading to the much faster kinetics. On the other hand, CONS also exhibited a higher extent of oxygen vacancy and structural defect, which would also enable the surface of CONS to be more active to react with MPS, resulting in a higher catalytic activity. Moreover, the unique shape of CONS also afforded much more contact surface, which would also allow CONS to quickly react with MPS to achieve the significantly high degradation kinetics.

3.3 Effect of catalyst dosage, MPS dosage and various Ensulizole concentrations

To further explore catalytic behaviors of these nanostructured Co_3O_4, the effects of catalyst and MPS dosages were then examined. Firstly, Fig. S5(a) and (b) reveal the effects of COCB and MPS concentration on Ensulizole degradation, respectively. In general, the degradation efficiency was greatly dependent on COCB and MPS concentration, and much higher COCB and MPS would certainly enhance Ensulizole degradation. Nevertheless, even though either 150 mg/L of COCB or MPS concentration was adopted, COCB could not completely eliminate Ensulizole, suggesting that COCB was certainly a less effective nanostructured Co_3O_4. Besides, Fig. S5(c) shows the effect of variation in COPL dosage on Ensulizole degradation. While COPL seemed much less effective than CONS, the slightly higher COPL dosage (150 mg/L) still enabled the very effective degradation of Ensulizole as $C_{60}/C_0 \sim 0$, with a faster $k = 0.059$ min^{-1} (See Table S2). On the other hand, Fig. S5(d) shows the effect of variation in MPS concentration on Ensulizole degradation, and a much higher MPS concentration (i.e., 150 mg/L) would also enable the almost complete elimination of Ensulizole.

Moreover, Fig. S5(e) shows the effect of CONS dosage, and, interestingly, even though the dosage of CONS was lowered to 50 mg/L, Ensulizole could be still quickly eliminated completely in 10 min. Nevertheless, the higher dosage of CONS would still enable an even faster degradation of Ensulizole as the k value at CONS = 150 mg/L would ramp substantially from 0.567 to 0.697 min^{-1}, whereas the k at CONS = 50 mg/L was relatively low as 0.434 min^{-1}. This indicates that the higher dosage of catalyst would certainly provide more reactive sites for reacting with MPS, leading to faster kinetics. On the other hand, when a relatively MPS was used (i.e., 50 mg/L), the incomplete degradation of Ensulizole was still observed even though CONS was applied. These comparative results demonstrate that CONS was certainly a much more advantageous Co_3O_4 than

the other two Co_3O_4; however, a sufficient amount of MPS was still required to achieve the full elimination of Ensulizole because ROS was produced from MPS rather than Co_3O_4.

3.4 Effects of temperature and pH on Ensulizole degradation

Since environmental conditions, such as temperature, and pH, would considerably influence MPS activation, the effects of temperature and pH on Ensulizole degradation would be then investigated to under how these Co_3O_4 behaved under various conditions. Firstly, Fig. 6(a) shows Ensulizole degradation by COCB-activated MPS at 30, 40 and 50 °C. When the temperature increased from 30 to 40 °C, the degradation efficiency was considerably enhanced as Ensulizole was almost completely eliminated in 60 min. In addition, the corresponding k would also increase from 0.0195 to 0.0411 min^{-1}. Furthermore, when temperature increased to 50 °C, Ensulizole could be completely eliminated in 45 min with a much faster k = 0.1265 min^{-1}. These results validate that the elevated temperature exhibited a significantly positive effect on Ensulizole degradation using COCB-activated MPS.

Fig. 6(d) then displays Ensulizole degradation by COPL at different temperatures. The elevated temperature also led to a huge enhancement in Ensulizole degradation as Ensulizole could be completely eliminated in 45 min at 40 °C, and 30 min at 50 °C. Thus, k could be tremendously increased from 0.0318 min^{-1} at 30 °C to 0.0964 min^{-1} at 40 °C, and 0.2323 min^{-1} at 50 °C, respectively, validating the positive effect of higher temperatures on Ensulizole degradation.

Moreover, in the case of CONS, while CONS had been very efficient to activate MPS for degrading Ensulizole rapidly, the elevated temperatures enabled the degradation to be even faster. The corresponding k value at 30 °C was 0.5665 min^{-1}, which can be further increased to 0.6659 min^{-1} at 40 °C, and 0.7215 min^{-1} at 50 °C, respectively.

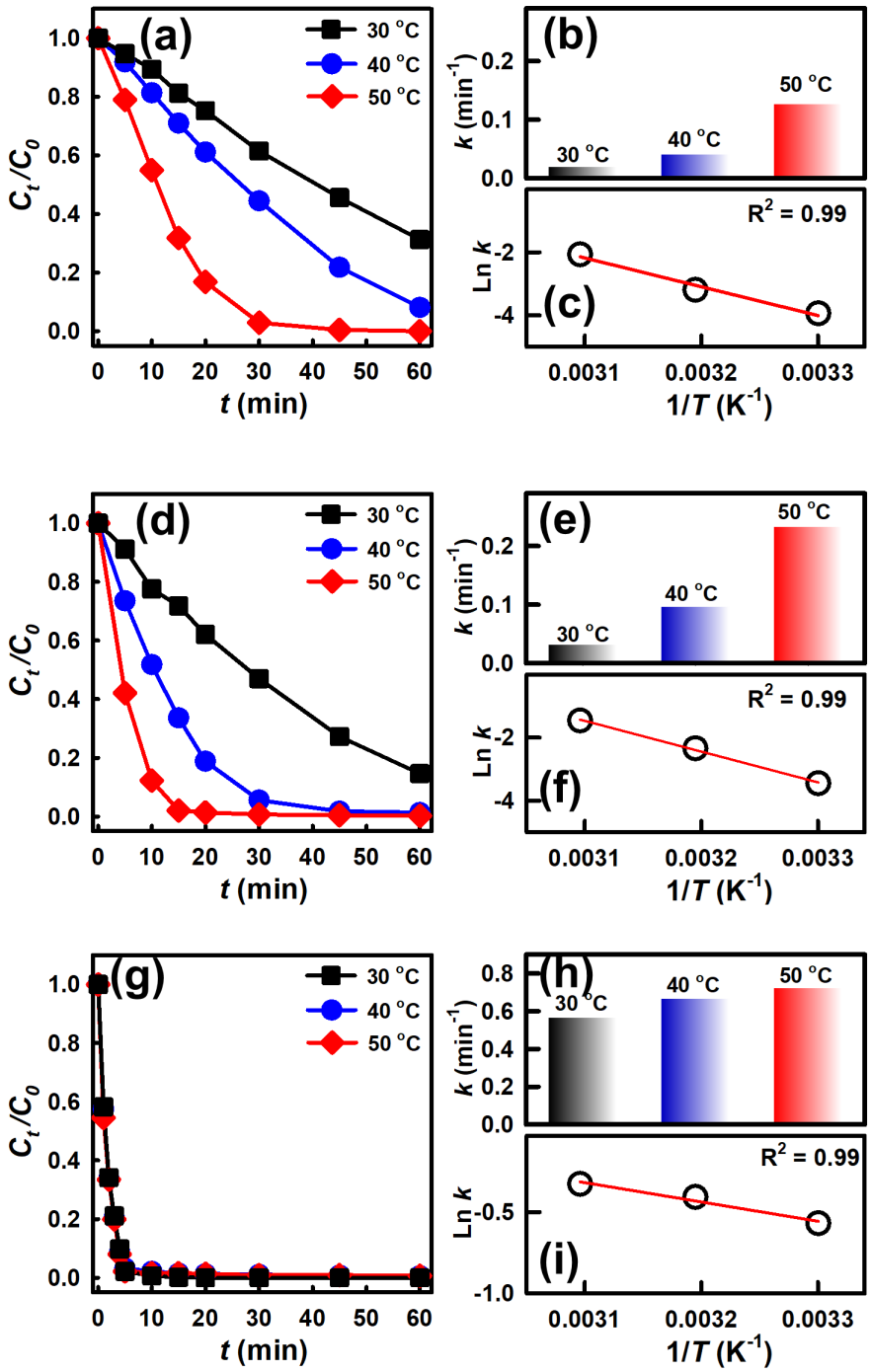

Fig. 6: Effect of temperature on Ensulizole degradation using MPS activated by nanostructured Co_3O_4: (a-c) COCB, (d-f) COPL, and (g-i) CONS
(Co_3O_4 catalysts = 100 mg/L, MPS = 100 mg/L, T = 30°C)

As the k value seemed to increase noticeably at higher temperatures by these three Co_3O_4 catalysts, it would be worthwhile to further interpret the relationship between k and temperature, which was then analyzed by using the Arrhenius equation as follows (Eq. (6)):

$$\mathrm{Ln}k - \ln A = -E_a/RT \quad (6)$$

where A denotes the pre-exponential factor, R means the universal gas constant, T indicates the reaction temperature in Kelvin (K), E_a denotes the activation energy (kJ/mol). Fig. 6(c), (f), and (i) display the plots of 1/T versus k using these three catalysts, respectively, and the data points in these three plots were all well fit by the linear regression, suggesting that the relationship between T and k of Ensulizole degradation could be properly described by the Arrhenius equation. Moreover, the slope of the fitting curve could be then adopted to calculate activation energy ~(kJ/mol) as summarized in Table S3. While COCB and COPL showed Ea values in the range of 75~80 kJ/mol, CONS exhibited a tremendously low E_a value of 9.8 kJ/mol, which was even much lower than E_a values by the reported catalysts in literatures. This ascertains that CONS was certainly a promising and unprecedented catalyst for activating MPS to degrade Ensulizole.

On the other hand, the effect of pH on Ensulizole degradation was also examined as shown in Fig. S6. Overall, the effect of pH on Ensulizole degradation using these three Co_3O_4 was quite comparable. The neutral condition (e.g., pH = 7) seemed the most favorable condition for Ensulizole degradation using these Co_3O_4, while the weakly basic (e.g., pH = 9) would slightly hinder Ensulizole degradation. This might be due to the fact that Ensulizole consists of a sulfonate group, and the basic condition would make the surface of Co_3O_4 more negatively charged, leading to a more intense repulsion between Ensulizole and Co_3O_4 under basic conditions. In addition, when the solution became even more basic (e.g., pH = 11), it would almost suppress Ensulizole degradation. This could be attributed to the fact that the highly basic condition would make MPS

more easily decompose without producing radicals, thereby suppressing Ensulizole degradation [52, 53].

On the other hand, the acidic environment (e.g., pH = 5) would also cause negative effects on Ensulizole degradation by using these three Co_3O_4, and the strongly acidic condition would cause even more adverse effect as MPS is prone to remaining very stable and less likely being activated under the acidic condition [53].

Nevertheless, CONS would still exhibit much higher degradation efficiencies even under the less favorable conditions, such as the weakly acidic and basic conditions, making it still the most advantageous catalyst among these three nanostructured Co_3O_4.

3.5 Effect of water sources, and the recyclability of CONS

As CONS was certainly a promising and much more powerful Co_3O_4 than COCB and COPL for activating MPS to degrade Ensulizole, the effect of water sources was also investigated to realize how different types of water would influence Ensulizole degradation by CONS-activated MPS. Fig. 7(a) shows Ensulizole degradation in seawater, tap water and DI water. In the case of seawater, the degradation kinetics seemed to be noticeably influenced as the corresponding k was decreased from 0.567 to 0.062 min^{-1}. This would be due to the fact that seawater contains a high concentration of NaCl as well as other ions, and especially, Cl- would react with $SO_4^{\bullet-}$ to form chloride radical species as follows (Eq. (7-8)) [54]:

$$Cl^- + SO_4^{\bullet-} \rightarrow Cl^{\bullet} + SO_4^{2-} \quad (7)$$

$$Cl^{\bullet} + Cl^- \rightarrow Cl_2^{\bullet-} \quad (8)$$

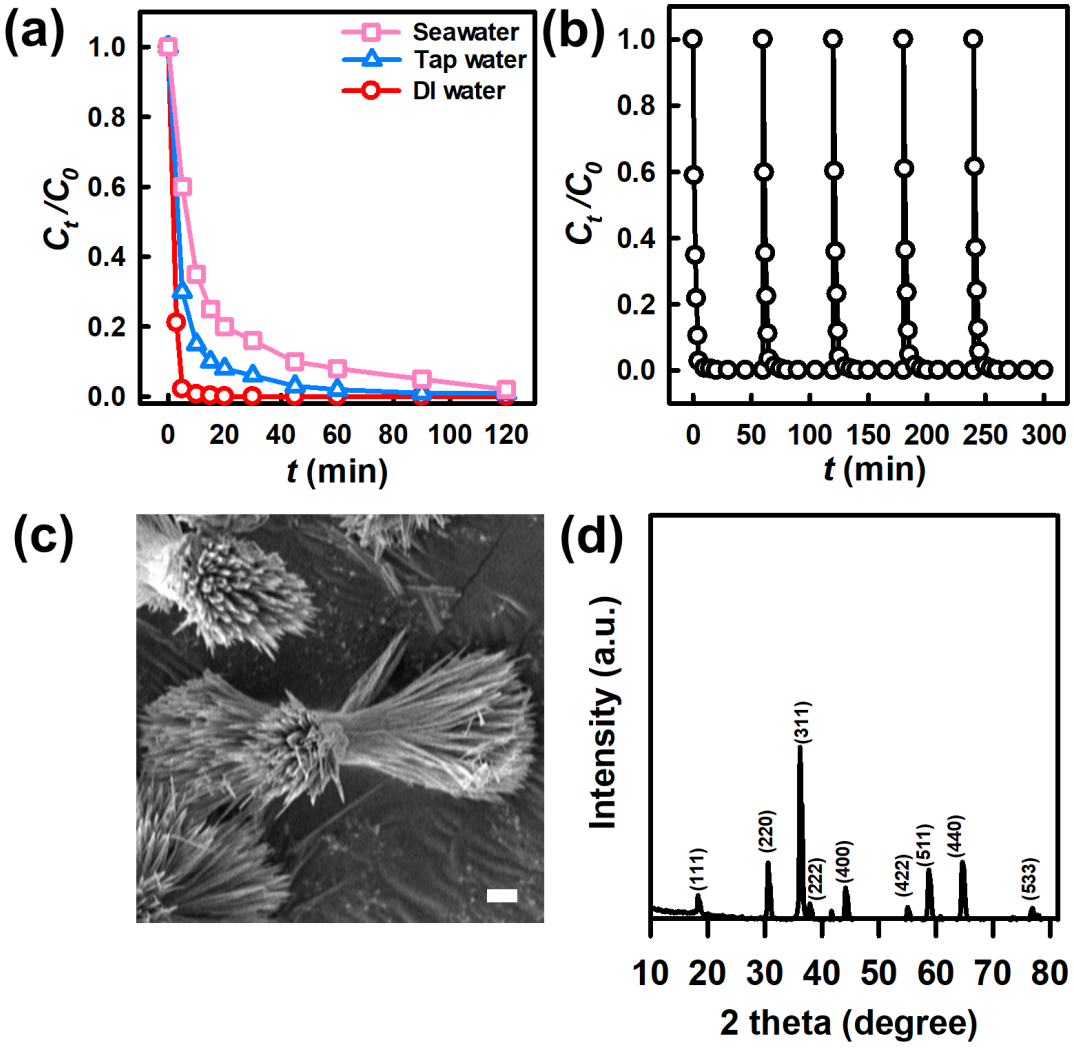

Fig. 7 (a) Effect of water type on Ensulizole degradation; (b) recyclability of CONS for Ensulizole degradation using MPS (CONS catalysts = 100 mg/L, MPS = 100 mg/L, T = 30°C); (c) SEM image (the scale bar = 1 μm), and (d) XRD pattern of used CONS

Unfortunately, the resultant chloride radicals (e.g., $Cl^{\bullet}$ (2.4V), $Cl_2^{\bullet-}$ (2.0V)) exhibit much lower oxidizing power than $SO_4^{\bullet-}$ (2.5-3.1 V), thereby hindering Ensulizole degradation. Nevertheless, Ensulizole even in seawater could be still completely eliminated by CONS-activated MPS in 120 min. On the other hand, Ensulizole in tap water was also evaluated, and Ensulizole degradation was also slightly influenced because the corresponding k was also decreased to 0.168 min^{-1}. This was because tap water generally contains chlorine which would also influence MPS activation and

then Ensulizole degradation. Nonetheless, CONS would still enable the complete elimination of Ensulizole, proving the effectiveness of CONS.

Furthermore, the recyclability of CONS was then further evaluated in Fig. 7(b), and Ensulizole could be completely and efficiently eliminated by the used CONS over the continuous five cycles. Moreover, the Co2p core-level spectrum of the used CONS was further analyzed. Fig. S7 shows that the positions of Co species in the used CONS were retained in comparison with the pristine CONS, proving the stability of CONS; however, the proportion of $Co^{2+}/_{(Co^{2+}+Co^{3+})}$ was changed (i.e., 60.11), indicating that there was electron transfer between Co^{2+} and Co^{3+} during the oxidation reaction. On the other hand, Fig. 7(c-d) also show the appearance and crystalline structure of the used CONS, which were very comparable to those of pristine CONS, demonstrating that CONS was reusable and stable catalyst, making it certainly a promising catalyst for activating MPS to eliminate Ensulizole. Moreover, the leaching test of Co ion during the experimental process was also investigated in this study. According to ICP-MS analysis, only 0.05 mg/L of Co ion has been detected in the solution over 5 degradation cycles, which is substantially lower than the initial concentration of CONS used in the experiment (i.e., 100 mg/L), indicating that Co was merely leached out in the solution during the experimental process. In order to verify the contribution of Co ions leached to MPS activation, homogeneous Co ions with the concentration of 0.05 mg/L were then used to activate MPS to degrade Ensulizole. As shown in Fig. S8, the concentration of Ensulizole was negligibly decreased after 60 min, demonstrating that the degradation of Ensulizole was mostly associated with the heterogeneous phase of cobalt in CONS.

3.6 Mechanism of CONS-activated MPS for Ensulizole degradation

To further probe in the mechanism of this promising CONS-activated MPS for Ensulizole degradation, several probing reagents were adopted to provide insights about reactive oxygen species derived from CONS-activted MPS. Firstly, tert-butyl alcohol (BuOH) was adopted as an inhibitor specifically for •OH, and Ensulizole degradation by CONS-activated MPS in the presence of BuOH was displayed in Fig. 8(a). Overall, the existence of BuOH caused a slight interference on Ensulizole degradation to decrease the k value from 0.567 to 0.195 min^{-1}, suggesting that •OH might exist and result from CONS-activated MPS.

On the other hand, the probing reagent, methanol (MeOH) was then evaluated as MeOH would inhibit both •OH and $SO_4^{\bullet-}$, and the degradation of Ensulizole by CONS-activated MPS was significantly suppressed in the presence of MeOH, signifying that MPS would be activated by CONS to generate radicals, including $SO_4^{\bullet-}$ as well as •OH.

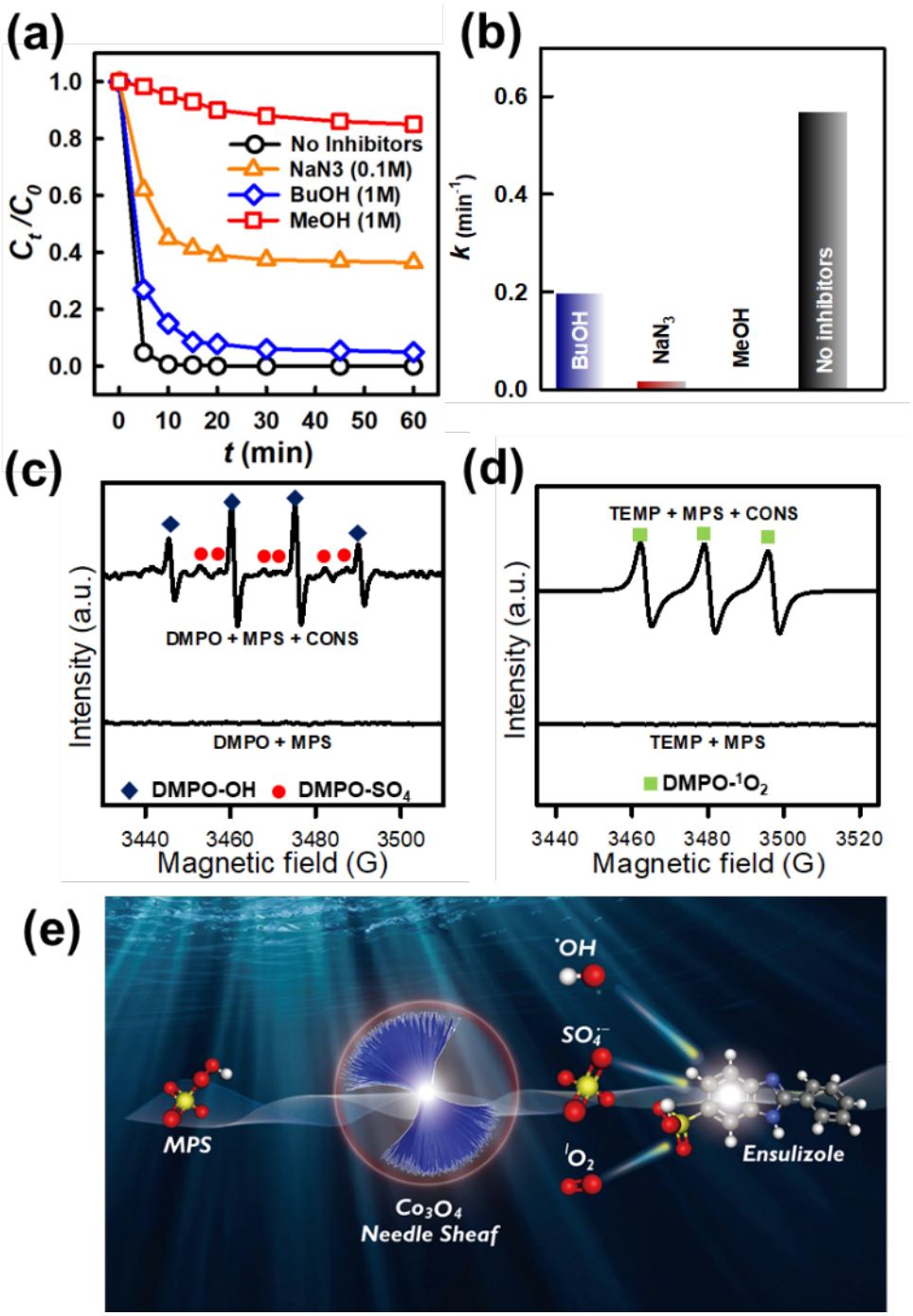

Fig. 8. (a) effect of radical inhibitors on Ensulizole degradation using CONS-activated MPS and (b) the calculated corresponding *k* values. (CONS = 100 mg/L, MPS = 100 mg/L, T = 30 °C, reaction time = 60 min); and (c-d) ESR analysis.

On the other hand, since MPS activation would also lead to the non-radical-route degradation by $^1O_2$ [9, 55, 56], it was important to verify if $^1O_2$ would be also present and derived from CONS-

activated MPS. Thus, a specific probing reagent for $^1O_2$, NaN_3, was tested, and the corresponding Ensulizole degradation was also noticeably inhibited as its *k* value was decreased to 0.016 min^{-1}, suggesting that $^1O_2$ shall also participate in Ensulizole degradation. Besides, different concentrations of these inhibitors have been further investigated. It can be noticed from Fig. S9 that Ensulizole was still effectively degraded by CONC-activated MPS in the presence of BuOH (5 M), which is similar with 0.5 M of BuOH, suggesting that 0.5 M of TBA was sufficient to quench all produced $^{\bullet}OH$ radicals. Moreover, in the presence of 0.5 M of NaN_3, the degradation of Ensulizole was slightly influenced compared to that of 0.1 M. On the other hand, when 5 M of MeOH was used, Ensulizole degradation was certainly inhibited as C_t/C_0 merely approached 0.95. These results indicated that $SO_4^{\bullet-}$, $^{\bullet}OH$, and $^1O_2$ were generated from CONS+MPS system to involve in the degradation of Ensulizole, and $SO_4^{\bullet-}$ is the dominant species contributing to the degradation of Ensulizole.

To elucidate occurrence of ROS from CONS-activated MPS, ESR analysis was adopted and displayed in Fig. 8(c), and (d). In the case of using DMPO as the spin-trapping compound, the combination of MPS, CONS and DMPO would afford the distinct pattern, which could be well-indexed to the oxidation adduct products of DMPO-SO_4 and DMPO-OH, confirming the occurrence of $SO_4^{\bullet-}$ and $^{\bullet}OH$ radicals from CONS-activated MPS, which contributed to Ensulizole degradation.

Moreover, in the case of using TEMP as the spin-trapping compound (Fig. 8(d)), the combination of MPS, CONS and TEMP would afford a triplet pattern, which would be well-indexed to TEMP-$^1O_2$, validating the existence of non-radical ROS and its contribution to Ensulizole degradation. Thus, Ensulizole degradation by CONS+MPS would be attributed to several ROS, such as $^{\bullet}OH$, $SO_4^{\bullet-}$, as well as $^1O_2$ as illustrated in Fig. 8(e).

3.7 Theoretic calculation, and a possible degradation process for Ensulizole

As CONS could lead to highly efficient degradation of Ensulizole, it was critical to investigate how Ensulizole was degraded by CONS-activated MPS. For assisting investigation, the density functional theory (DFT) calculation was utilized to offer important theoretical information about Ensulizole for understanding how Ensulizole would be attacked by these ROS. The details of DFT calculation about Ensulizole was given in the supporting information to optimize the geometry of Ensulizole, and calculate Fukui indices, molecule orbitals (MO) as well as electrostatic potential mapping analysis.

Fig. 9(a) reveals the optimized geometry of Ensulizole with its MOs (Fig. 9(c)). As the semi-transparent green, and red zones signified electron-deficient, and electron-rich zones of Ensulizole. In particular, the HOMO of Ensulizole's imidazole ring would tend to release electrons; consequently, Ensulizole was prone to receiving attacks from electrophilic ROS, such as, $^{\bullet}OH$, and, $SO_4^{\bullet-}$. Fig. 9(b) also summarizes Fukui indices (i.e., F^-, F^0, and F^+) of each site in Ensulizole, and a specific site with a much higher Fukui index (F^-) was prone to drawing radical attacks. Among these sites, the 6N site exhibited the highest F- value, followed by 19C site, 7C site, 9C site, and then 11C site. In addition, sites with relatively high F^0 values would also withdraw non-radical attacks. Therefore, 6N, 9C as well 19C also appeared as relatively active sites to receive attacks. As a result, Ensulizole degradation might be started by attacking N6 site to decompose the entire molecule of Ensulizole into phenolic intermediates, which would receive further attacks on sites, such as C11 or C19 for further decomposition. Besides, the ESP of Ensulizole (Fig. 9(d)) also indicates that N6, C11, and C19 would tend to receive radicals, leading to the decomposition.

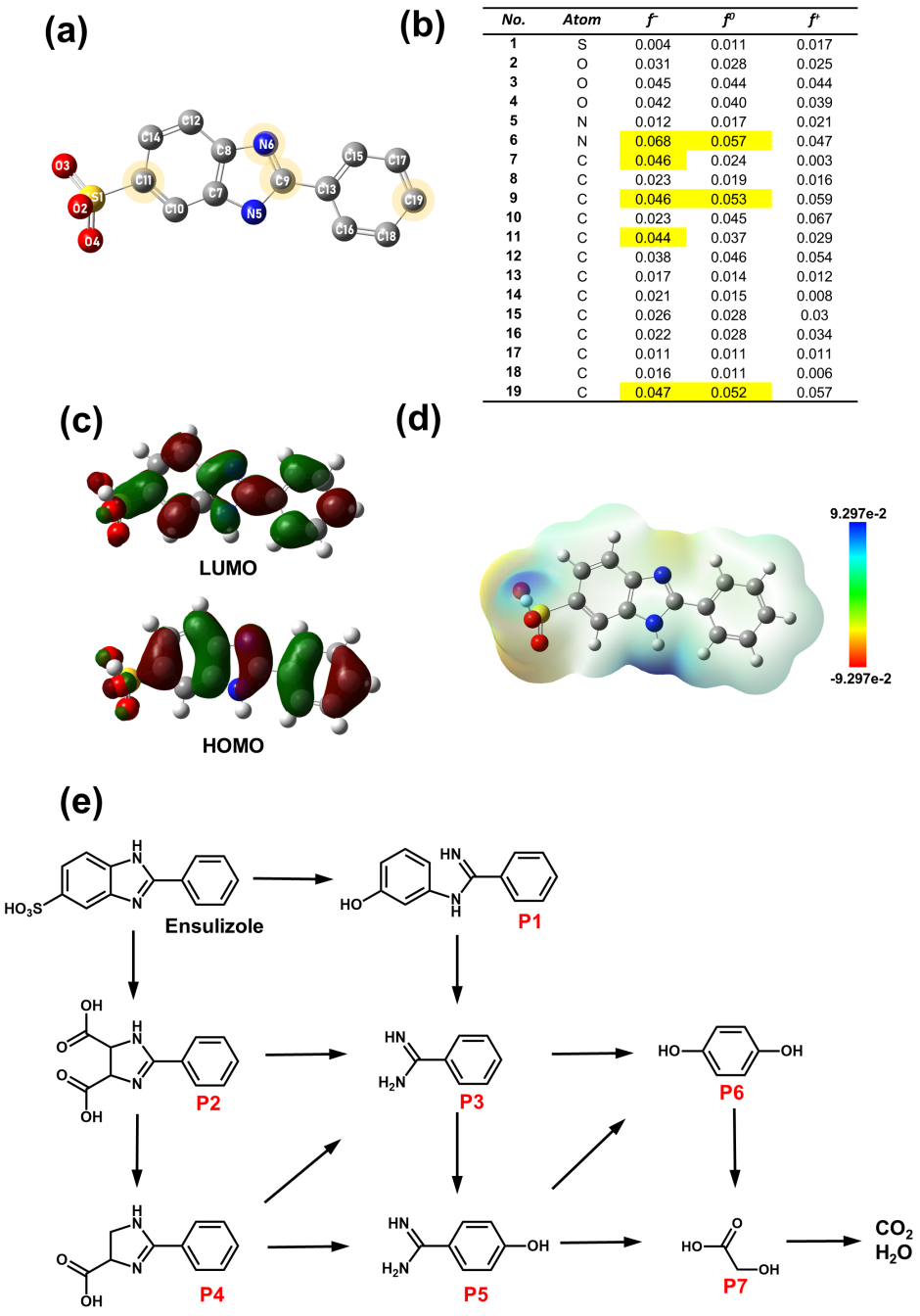

No.	Atom	f^-	f^0	f^+
1	S	0.004	0.011	0.017
2	O	0.031	0.028	0.025
3	O	0.045	0.044	0.044
4	O	0.042	0.040	0.039
5	N	0.012	0.017	0.021
6	N	0.068	0.057	0.047
7	C	0.046	0.024	0.003
8	C	0.023	0.019	0.016
9	C	0.046	0.053	0.059
10	C	0.023	0.045	0.067
11	C	0.044	0.037	0.029
12	C	0.038	0.046	0.054
13	C	0.017	0.014	0.012
14	C	0.021	0.015	0.008
15	C	0.026	0.028	0.03
16	C	0.022	0.028	0.034
17	C	0.011	0.011	0.011
18	C	0.016	0.011	0.006
19	C	0.047	0.052	0.057

Fig. 9. Theoretical analysis for Ensulizole molecule: (a) Ensulizole; (b) Fukui index distributions; (c) molecular orbitals; (d) Electrostatic potential-mapped molecular surface of Ensulizole; (e) A probable degradation process of Ensulizole degradation.

Next, for unveiling the degradation pathway of Ensulizole by CONS-activated MPS, its degradation by-products were then analyzed, and several noticeable intermediates were

summarized in Table S4. Based on these noticeable intermediates, a possible degradation pathway for Ensulizole by CONS-activated MPS could be then depicted in Fig. 9(e). Initially, Ensulizole would be attacked to break the imidazole ring, resulting in an intermediate, P1, which might be further decomposed to generate P3. On the other hand, the phenolic group connecting to the sulfonate group might be also attacked and opened to generate the intermediate, P2, which would be then further oxidized to generate another intermediate, P4. Both P3 and P4 might be oxidized to produce P5, while P3 could be also oxidized to afford P6. Next, these intermediates, such as P5 and P6, would be further decomposed to produce much smaller molecules, including P7, and eventually to CO_2 and H_2O.

4. Conclusion

For developing an effective Co-based catalyst for activating MPS to degrade one of the most common sunscreen protecting agents, Ensulizole, in water, three Co_3O_4 materials with distinct nanostructures and shapes were fabricated, including Co_3O_4 cone ball (COCB), Co_3O_4 plate lump (COPL), and Co_3O_4 needle sheaf (CONS). Apart from the distinct shapes in these nanostructured Co_3O_4 catalysts, their surficial properties were also noticeably different with different fractions of Co^{2+}, and Co^{3+}, various oxygen vacancies, textural features and surface defects. Through comparing these three nanostructured Co_3O_4 for activating MPS to degrade Ensulizole, the relationship between shapes, surficial properties and nanostructures of Co_3O_4, and catalytic activities for MPS activation can be unveiled. In particular, since CONS contained a higher fraction of Co^{2+}, oxygen vacancies, more surface defects, as well as much higher surface area, CONS exhibited the tremendously higher catalytic activity than COCB and COPL for activating MPS to eliminate Ensulizole completely and rapidly. Moreover, the Ea value of Ensulizole

degradation of CONS was significantly low as 9.8 kJ/mol, which was the lowest Ea ever reported in literatures, making CONS a truly promising Co_3O_4 for activating MPS to Ensulizole, possibly owing to its much reactive surface. CONS could also retain its catalytic activities over 5 continuous cycles to efficiently and rapidly degrade Ensulizole. The activation mechanism of MPS by CONS and Ensulizole degradation pathway were also comprehensively elucidated via experimental evidences as well as the theoretical (DFT) calculation to offer insightful information of development of Co-based heterogeneous catalysts for Ensulizole degradation.

References:

[1] A. Khamkeaw, M. Phisalaphong, B. Jongsomjit, K.Y.A. Lin, A.C.K. Yip, Synthesis of mesoporous MFI zeolite via bacterial cellulose-derived carbon templating for fast adsorption of formaldehyde.

[2] A. Wick, G. Fink, T.A. Ternes, Comparison of electrospray ionization and atmospheric pressure chemical ionization for multi-residue analysis of biocides, UV-filters and benzothiazoles in aqueous matrices and activated sludge by liquid chromatography-tandem mass spectrometry, J Chromatogr A, 1217 (2010) 2088-2103.

[3] A. Al-Anazi, W.H. Abdelraheem, C. Han, M.N. Nadagouda, L. Sygellou, M.K. Arfanis, P. Falaras, V.K. Sharma, D.D. Dionysiou, Cobalt ferrite nanoparticles with controlled composition-peroxymonosulfate mediated degradation of 2-phenylbenzimidazole-5-sulfonic acid, Appl Catal B, 221 (2018) 266-279.

[4] X. Zhang, M. Feng, L. Wang, R. Qu, Z. Wang, Catalytic degradation of 2-phenylbenzimidazole-5-sulfonic acid by peroxymonosulfate activated with nitrogen and sulfur co-doped CNTs-COOH loaded CuFe2O4, Chemical Engineering Journal, 307 (2017) 95-104.

[5] L. Hernandez-Leal, H. Temmink, G. Zeeman, C.J. Buisman, Removal of micropollutants from aerobically treated grey water via ozone and activated carbon, Water Res, 45 (2011) 2887-2896.

[6] K. Fisch, J.J. Waniek, D.E. Schulz-Bull, Occurrence of pharmaceuticals and UV-filters in riverine run-offs and waters of the German Baltic Sea, Mar Pollut Bull, 124 (2017) 388-399.

[7] M.-C. Li, F. Ghanbari, F.-C. Chang, C. Hu, K.-Y.A. Lin, Y. Du, Enhanced degradation of 5-sulfosalicylic acid using peroxymonosulfate activated by ordered porous silica-confined Co3O4 prepared via a solvent-free confined space strategy, Separation and Purification Technology, (2020) 116972.

[8] W. Li, S. Li, Y. Tang, X. Yang, W. Zhang, X. Zhang, H. Chai, Y. Huang, Highly efficient activation of peroxymonosulfate by cobalt sulfide hollow nanospheres for fast ciprofloxacin degradation, Journal of Hazardous Materials, 389 (2020) 121856.

[9] P. Liang, C. Zhang, X. Duan, H. Sun, S. Liu, M.O. Tade, S. Wang, An insight into metal organic framework derived N-doped graphene for the oxidative degradation of persistent contaminants: formation mechanism and generation of singlet oxygen from peroxymonosulfate, Environmental Science: Nano, 4 (2017) 315-324.
[10] K.-Y.A. Lin, H.-A. Chang, Zeolitic Imidazole Framework-67 (ZIF-67) as a heterogeneous catalyst to activate peroxymonosulfate for degradation of Rhodamine B in water, J Taiwan Inst Chem Eng, 53 (2015) 40-45.
[11] K.-Y.A. Lin, J.-T. Lin, A.P. Jochems, Oxidation of amaranth dye by persulfate and peroxymonosulfate activated by ferrocene, Journal of Chemical Technology & Biotechnology, 92 (2017) 163-172.
[12] K.-Y.A. Lin, Z.-Y. Zhang, Degradation of Bisphenol A using peroxymonosulfate activated by one-step prepared sulfur-doped carbon nitride as a metal-free heterogeneous catalyst, Chemical Engineering Journal, 313 (2017) 1320-1327.
[13] P. Hu, M. Long, Cobalt-catalyzed sulfate radical-based advanced oxidation: A review on heterogeneous catalysts and applications, Applied Catalysis B: Environmental, 181 (2016) 103-117.
[14] Y. Guo, D.C.W. Tsang, X. Zhang, X. Yang, Cu(II)-catalyzed degradation of ampicillin: effect of pH and dissolved oxygen, Environmental Science and Pollution Research, 25 (2018) 4279-4288.
[15] S.-N. Zhu, C. Wang, A.C.K. Yip, D.C.W. Tsang, Highly effective degradation of sodium dodecylbenzene sulphonate and synthetic greywater by Fenton-like reaction over zerovalent iron-based catalyst, Environmental Technology, 36 (2015) 1423-1432.
[16] M.-H. Li, K.-Y.A. Lin, M.-T. Yang, B.X. Thanh, D.C.W. Tsang, Prussian Blue Analogue-derived co/fe bimetallic nanoparticles immobilized on S/N-doped carbon sheet as a magnetic heterogeneous catalyst for activating peroxymonosulfate in water, Chemosphere, 244 (2020) 125444.
[17] J.-Y. Yin, H. Wang, K.-P. Yu, J. Lee, K.-Y.A. Lin, Degradation of sunscreen agent 2-phenylbenzimidazole-5-sulfonic acid using monopersulfate activated by MOF-derived cobalt sulfide nanoplates, Journal of Water Process Engineering, 44 (2021) 102282.
[18] G.P. Anipsitakis, E. Stathatos, D.D. Dionysiou, Heterogeneous Activation of Oxone Using Co3O4, The Journal of Physical Chemistry B, 109 (2005) 13052-13055.
[19] D.D. Tuan, C. Hung, W. Da Oh, F. Ghanbari, J.-Y. Lin, K.-Y. Andrew Lin, Porous Hexagonal Nanoplate Cobalt Oxide derived from a Coordination Polymer as an Effective Catalyst for activating Oxone in Water, Chemosphere, (2020) 127552.
[20] M.-W. Zhang, M.-T. Yang, S. Tong, K.-Y.A. Lin, Ferrocene-modified iron-based metal-organic frameworks as an enhanced catalyst for activating oxone to degrade pollutants in water, Chemosphere, 213 (2018) 295-304.
[21] K.-Y.A. Lin, T.-Y. Lin, Degradation of Acid Azo Dyes Using Oxone Activated by Cobalt Titanate Perovskite, Water, Air, & Soil Pollution, 229:10 (2018).
[22] K.-Y.A. Lin, J.-T. Lin, X.-Y. Lu, C. Hung, Y.-F. Lin, Electrospun magnetic cobalt-embedded carbon nanofiber as a heterogeneous catalyst for activation of oxone for degradation of Amaranth dye, Journal of Colloid and Interface Science, 505 (2017) 728-735.
[23] Q. Yang, H. Choi, S.R. Al-Abed, D.D. Dionysiou, Iron–cobalt mixed oxide nanocatalysts: Heterogeneous peroxymonosulfate activation, cobalt leaching, and ferromagnetic properties for environmental applications, Applied Catalysis B: Environmental, 88 (2009) 462-469.

[24] C. Cai, H. Zhang, X. Zhong, L. Hou, Ultrasound enhanced heterogeneous activation of peroxymonosulfate by a bimetallic Fe–Co/SBA-15 catalyst for the degradation of Orange II in water, Journal of Hazardous Materials, 283 (2015) 70-79.
[25] X. Chen, J. Chen, X. Qiao, D. Wang, X. Cai, Performance of nano-Co3O4/peroxymonosulfate system: Kinetics and mechanism study using Acid Orange 7 as a model compound, Applied Catalysis B: Environmental, 80 (2008) 116-121.
[26] C. Wang, P. Shi, X. Cai, Q. Xu, X. Zhou, X. Zhou, D. Yang, J. Fan, Y. Min, H. Ge, W. Yao, Synergistic Effect of Co3O4 Nanoparticles and Graphene as Catalysts for Peroxymonosulfate-Based Orange II Degradation with High Oxidant Utilization Efficiency, The Journal of Physical Chemistry C, 120 (2016) 336-344.
[27] C.Y. Ma, Z. Mu, J.J. Li, Y.G. Jin, J. Cheng, G.Q. Lu, Z.P. Hao, S.Z. Qiao, Mesoporous Co3O4 and Au/Co3O4 Catalysts for Low-Temperature Oxidation of Trace Ethylene, Journal of the American Chemical Society, 132 (2010) 2608-2613.
[28] Y. Sun, J. Liu, J. Song, S. Huang, N. Yang, J. Zhang, Y. Sun, Y. Zhu, Exploring the Effect of Co3O4 Nanocatalysts with Different Dimensional Architectures on Methane Combustion, 8 (2016) 540-545.
[29] X. Xie, Y. Li, Z.-Q. Liu, M. Haruta, W. Shen, Low-temperature oxidation of CO catalysed by Co3O4 nanorods, Nature, 458 (2009) 746-749.
[30] D.D. Tuan, C. Hu, E. Kwon, Y. Du, K.-Y.A. Lin, Coordination polymer-derived porous Co3O4 nanosheet as an effective catalyst for activating peroxymonosulfate to degrade sulfosalicylic acid, Applied Surface Science, 532 (2020) 147382.
[31] W.-C. Yun, K.-Y.A. Lin, W.-C. Tong, Y.-F. Lin, Y. Du, Enhanced degradation of paracetamol in water using sulfate radical-based advanced oxidation processes catalyzed by 3-dimensional Co3O4 nanoflower, Chemical Engineering Journal, 373 (2019) 1329-1337.
[32] X.-Y. Yu, Q.-Q. Meng, T. Luo, Y. Jia, B. Sun, Q.-X. Li, J.-H. Liu, X.-J. Huang, Facet-dependent electrochemical properties of Co3O4 nanocrystals toward heavy metal ions, Scientific Reports, 3 (2013) 2886.
[33] G. Cheng, T. Kou, J. Zhang, C. Si, H. Gao, Z. Zhang, O22-/O- functionalized oxygen-deficient Co3O4 nanorods as high performance supercapacitor electrodes and electrocatalysts towards water splitting, Nano Energy, 38 (2017) 155-166.
[34] D. Wang, Q. Wang, T. Wang, Morphology-Controllable Synthesis of Cobalt Oxalates and Their Conversion to Mesoporous Co3O4 Nanostructures for Application in Supercapacitors, Inorganic Chemistry, 50 (2011) 6482-6492.
[35] Q. Ren, S. Mo, R. Peng, Z. Feng, M. Zhang, L. Chen, M. Fu, J. Wu, D. Ye, Controllable synthesis of 3D hierarchical Co3O4 nanocatalysts with various morphologies for the catalytic oxidation of toluene, Journal of Materials Chemistry A, 6 (2018) 498-509.
[36] Z. Sun, T. Liao, L. Kou, Strategies for designing metal oxide nanostructures, Science China Materials, 60 (2017) 1-24.
[37] Z.H. Ibupoto, S. Elhag, M.S. AlSalhi, O. Nur, M. Willander, Effect of Urea on the Morphology of Co3O4 Nanostructures and Their Application for Potentiometric Glucose Biosensor, Electroanalysis, 26 (2014) 1773-1781.
[38] D. Guragain, C. Zequine, T. Poudel, D. Neupane, R.K. Gupta, S.R. Mishra, Influence of Urea on the Synthesis of NiCo2O4 Nanostructure: Morphological and Electrochemical Studies, Journal of Nanoscience and Nanotechnology, 20 (2020) 2526-2537.

[39] T. Fuchigami, R. Kimata, M. Haneda, K.-i. Kakimoto, Complex Three-Dimensional Co3O4 Nano-Raspberry: Highly Stable and Active Low-temperature CO Oxidation Catalyst, Nanomaterials, 8 (2018) 662.
[40] H.-K. Lai, Y.-Z. Chou, M.-H. Lee, K.-Y.A. Lin, Coordination polymer-derived cobalt nanoparticle-embedded carbon nanocomposite as a magnetic multi-functional catalyst for energy generation and biomass conversion, Chemical Engineering Journal, 332 (2018) 717-726.
[41] K.-Y.A. Lin, B.-J. Chen, Magnetic carbon-supported cobalt derived from a Prussian blue analogue as a heterogeneous catalyst to activate peroxymonosulfate for efficient degradation of caffeine in water, Journal of Colloid and Interface Science, 486 (2017) 255-264.
[42] L.-L. Feng, M. Fan, Y. Wu, Y. Liu, G.-D. Li, H. Chen, W. Chen, D. Wang, X. Zou, Metallic Co9S8 nanosheets grown on carbon cloth as efficient binder-free electrocatalysts for the hydrogen evolution reaction in neutral media, Journal of Materials Chemistry A, 4 (2016) 6860-6867.
[43] S. Zhao, F. Hu, J. Li, Hierarchical Core–Shell Al2O3@Pd-CoAlO Microspheres for Low-Temperature Toluene Combustion, ACS Catalysis, 6 (2016) 3433-3441.
[44] B. de Rivas, R. López-Fonseca, C. Jiménez-González, J.I. Gutiérrez-Ortiz, Synthesis, characterisation and catalytic performance of nanocrystalline Co3O4 for gas-phase chlorinated VOC abatement, Journal of Catalysis, 281 (2011) 88-97.
[45] Q. Liu, L.-C. Wang, M. Chen, Y. Cao, H.-Y. He, K.-N. Fan, Dry citrate-precursor synthesized nanocrystalline cobalt oxide as highly active catalyst for total oxidation of propane, Journal of Catalysis, 263 (2009) 104-113.
[46] X. Wang, Y. Liu, T. Zhang, Y. Luo, Z. Lan, K. Zhang, J. Zuo, L. Jiang, R. Wang, Geometrical-Site-Dependent Catalytic Activity of Ordered Mesoporous Co-Based Spinel for Benzene Oxidation: In Situ DRIFTS Study Coupled with Raman and XAFS Spectroscopy, ACS Catalysis, 7 (2017) 1626-1636.
[47] L. Hu, Q. Peng, Y. Li, Selective Synthesis of Co3O4 Nanocrystal with Different Shape and Crystal Plane Effect on Catalytic Property for Methane Combustion, Journal of the American Chemical Society, 130 (2008) 16136-16137.
[48] N.H. Trang, E. Kwon, G. Lisak, C. Hu, K.-Y. Andrew Lin, Cobalt ferrite nanoparticle-loaded nitrogen-doped carbon sponge as a magnetic 3D heterogeneous catalyst for monopersulfate-based oxidation of salicylic acid, Chemosphere, 267 (2021) 128906.
[49] Y. Bao, W.-D. Oh, T.-T. Lim, R. Wang, R.D. Webster, X. Hu, Elucidation of stoichiometric efficiency, radical generation and transformation pathway during catalytic oxidation of sulfamethoxazole via peroxymonosulfate activation, Water Research, 151 (2019) 64-74.
[50] Q.F. Wang, Y.S. Shao, N.Y. Gao, W.H. Chu, J.X. Chen, X. Lu, Y.P. Zhu, N. An, Activation of peroxymonosulfate by Al2O3-based CoFe2O4 for the degradation of sulfachloropyridazine sodium: Kinetics and mechanism, Sep Purif Technol, 189 (2017) 176-185.
[51] P.D. Hu, M.C. Long, Cobalt-catalyzed sulfate radical-based advanced oxidation: A review on heterogeneous catalysts and applications, Appl Catal B-Environ, 181 (2016) 103-117.
[52] A. Rastogi, S.R. Al-Abed, D.D. Dionysiou, Sulfate radical-based ferrous–peroxymonosulfate oxidative system for PCBs degradation in aqueous and sediment systems, Applied Catalysis B: Environmental, 85 (2009) 171-179.
[53] W. Guo, S. Su, C. Yi, Z. Ma, Degradation of antibiotics amoxicillin by Co3O4-catalyzed peroxymonosulfate system, Environmental Progress & Sustainable Energy, 32 (2013) 193-197.

[54] C. Tan, N. Gao, Y. Deng, J. Deng, S. Zhou, J. Li, X. Xin, Radical induced degradation of acetaminophen with Fe3O4 magnetic nanoparticles as heterogeneous activator of peroxymonosulfate, Journal of Hazardous Materials, 276 (2014) 452-460.
[55] R. Luo, M. Li, C. Wang, M. Zhang, M.A. Nasir Khan, X. Sun, J. Shen, W. Han, L. Wang, J. Li, Singlet oxygen-dominated non-radical oxidation process for efficient degradation of bisphenol A under high salinity condition, Water Research, 148 (2019) 416-424.
[56] S. Yang, P. Wu, J. Liu, M. Chen, Z. Ahmed, N. Zhu, Efficient removal of bisphenol A by superoxide radical and singlet oxygen generated from peroxymonosulfate activated with Fe0-montmorillonite, Chemical Engineering Journal, 350 (2018) 484-495.